EAST EUROPEAN JOURNAL OF PHYSICS. 4. 159–176 (2024)
DOI: 10.26565/2312-4334-2024-4-15 ISSN 2312-4334

A BIOMAGNETIC COUPLE STRESS FLUID FLOW IN AN ANISOTROPIC POROUS CHANNEL WITH STRETCHING WALLS

R. Vijaya Sree[a, b], **V. Krishna Narla**[b*], **K. Suresh Babu**[c]
[a] *ACE Engineering College, Department of Mathematics, Hyderabad, Telangana, 501301, India.*
[b] *GITAM Deemed to be University, Department of Mathematics, Hyderabad, 502329, India.*
[c] *Gokaraju Rangaraju Institute of Engineering & Technology, Department of Mathematics, Hyderabad, 500090, India.*
[*] *Corresponding Author e-mail: vnarla@gitam.edu*
Received September 2, 2024; revised November 8, 2024; accepted November 18, 2024

The present study investigates the dynamics of a biomagnetic couple stress fluid within an anisotropic porous channel where the channel walls are stretchable. This study examines the flow behavior under the influence of an external magnetic field generated by a magnetic dipole. Appropriate dimensionless parameters are introduced to simplify the equations of the problem. A suitable numerical approach based on the Spectral Quasi-Linearization Method is utilized to obtain a solution to the problem. In this work, influence of several important parameters like the anisotropic permeability ratio, couple stress parameter, anisotropic angle, Darcy number, ferromagnetic interaction parameter, Reynolds number, and Prandtl number are examined. The results indicate that ferromagnetic interaction parameter and couple stress parameter significantly impact heat transfer and fluid flow. Permeability ratio and angle also affect the flow dynamics. Furthermore, the coefficient of skin friction and rate of heat transfer were examined, varying the couple stress and ferromagnetic interaction parameters. The findings demonstrate that an existence of magnetic dipole and anisotropic permeability significantly influences the flow and thermal properties of ferrofluids, providing valuable insights for optimizing heat transfer and controlling fluid flow in diverse engineering and medical applications.

Keywords: *Couple stress fluid; Magnetic dipole; Anisotropic porous media; Anisotropic permeability; Heat transfer; Spectral Quasi-Linearization method*

PACS: 47.50.-d; 47.65.Cb; 47.35.Tv; 47.56.+r; 44.30.+v; 44.15.+a; 02.70.Hm

1. INTRODUCTION

The research on biomagnetic ferrofluids has gained remarkable significance in recent times owing to their distinctive characteristics and possible uses in diverse domains including biomedical engineering, pharmaceutical administration, and thermal transport systems [1]. A key area of interest in biomagnetic ferrofluid research is understanding the behaviour of these fluids when subjected to a magnetic dipole, especially in confined geometries such as channels with stretching walls. The stretching walls introduce a shear force, which can significantly influence the flow dynamics within the channel. Understanding these interactions is crucial for optimizing the design and operation of devices that utilize biomagnetic fluids, particularly in processes where efficient heat transfer and fluid control are essential like applications related to engineering, biomedicine, and materials science [2, 3]. Ferrofluids demonstrate controllable flow behaviour and enhanced thermal conductivity under magnetic influence, and have a range of fascinating applications across various fields which include magnetic resonance imaging (MRI) enhancement, drug delivery systems, cooling systems, magnetic separation and filtering, optical devices, magnetic sensors and actuators [4]–[7]. A mathematical model of magnetic field-induced blood flow was developed by E.E. Tzirtzilakis [8]. The magnetic dipole-induced dynamics of visco-elastic fluid were examined by Misra and Shit [9, 10]. They examined the variation in the velocity of blood with respect to a magnetic field, viscoelastic parameter and thermal diffusivity using the method of finite difference. They concluded that by enhancing the intensity of magnetic force field, regulation of wall temperature can be achieved by eliminating occurrence of flow reversal. An observation was made that larger magnetic strength corresponds to higher temperature. The applicability of these analyses was demonstrated by studying blood flow in arteries within walls, which are stretchable. A second-grade electrically conducting fluid, which is both steady and incompressible, was investigated by Misra et al. [11] in channel while a transverse uniform magnetic field was present. All the studies carried out by Misra et al. are driven by various potential uses in the biomedical engineering domain. Couple stress fluids, which are a particular category of non-Newtonian fluids, have a nonsymmetric stress tensor and microstructure in their fluid structure, which makes them defy the Newtonian fluid theory. Stokes[12] developed the theory of couple stress fluids in 1966, expanding classical fluid mechanics to account for couple stresses. Because of their potential applications in a wide range of fluid flow systems, couple stress fluids have garnered significant interest from many researchers [13]–[15]. Ramesh [16] examined the propagation of a couple stress fluid having peristaltic behaviour, in an inclined asymmetrical porous channel. It was noted in the study that the pressure gradient declines as the Reynolds number and the channel's angle of inclination are raised. Studies have shown that the heat transfer and temperature exhibit positive correlations with the Darcy number and also

Cite as: R. Vijaya Sree, V.K. Narla, K. Suresh Babu, East Eur. J. Phys. 4, 159 (2024), https://doi.org/10.26565/2312-4334-2024-4-15

angle of inclination. A study conducted by Ramanamurthy and Pavan Kumar [17] examined couple stress fluid flow in a channel of rectangular shape formed due to a magnetic field applied transversely. Some more studies on couple stress fluids and power-law fluids which are subjected to magnetic field can be found in [18]–[22]. In their study, Nadeem et al. [23] analysed impact of nanoparticles on magnetohydrodynamic (MHD) flow of a Casson fluid over an exponentially permeable shrinking sheet. Coupled stress fluids in curved porous channels were investigated by Pramod et al.[24]. The flow governing equations, which are highly non-linear, were solved by HAM(Homotopy Analysis Method). They concluded that when compared with the Newtonian fluids, for couple stress fluids the magnitude of velocity and temperature profiles are smaller. Ishaq et al. [25] investigated the behaviour of couple stress fluid traversing a porous slit which is linear in a Darcy porous media. The flow was considered creeping and the solution was obtained using an Inverse method technique. Their research explored kidney disease's impact on renal tubule fluid flow, highlighting potential clogging by fibers, lipids, and waste particles, aiding in disease management and improving renal medicine development. Using a Boussinesq couple stress fluid, Patra et al. [26] analysed the characteristics of flow across a stretched sheet in porous media. The flow was exposed to varying magnetic fields and thermal radiation. An order-4 RK method was applied to obtain the solution numerically. They discovered that the distributions of velocity and temperature were impacted by parameters like Darcy number, magnetic field strength, and couple stress parameter. Recent advanced research has primarily focused on developing effective numerical methods to solve the intricate, nonlinear differential equations that govern fluid flow dynamics. To linearise and solve nonlinear terms with high accuracy, one such method is Spectral Quasi-Linearization Method (SQLM), which combines the Quasilinearization technique with spectral methods. Numerous fluid flow applications, such as the investigation of flows across boundary layer over stretching/shrinking sheets in non-Darcy porous media, have benefited from the successful application of this technique [27]–[29]. With a focus on nanofluid flow, Rai and Mondal [30] examined modern spectral approaches for solving nonlinear fluid flow problems. It consists of various spectral-based techniques such as Spectral Quasi-Linearization (SQLM), spectral relaxation (SRM), and spectral local linearisation (SLLM) which are most effective and precise than finite difference methods, in solving both ordinary and partial differential equations.

Most studies on ferrofluid flow dynamics and heat transfer do not take into account the impact of coupled stress fluid dynamics, magnetic dipoles, and anisotropic porous medium. Using a mathematical model and solving the governing equations, this work aims to elucidate the impact of the interaction among magnetic dipole, stretching walls, anisotropic permeability and ferrofluid characteristics on the system's overall performance. The flow governing equations, which take into account couple stresses and magnetic forces, are numerically solved by applying Spectral Quasi-Linearization Method (SQLM), after making similarity transformations. Our study examines how the key parameters, including couple stress, ferromagnetic interaction, Prandtl number, Reynolds number, Darcy number, anisotropic permeability, and angle affect velocity and temperature profiles in boundary layers. The findings give a thorough understanding of the intricate interactions between these variables and show how they impact the flow and thermal properties of ferrofluids. The results demonstrate the method's resilience and efficacy in handling challenging fluid dynamics applications by providing insightful guidance for optimising heat transfer and flow control in various engineering applications involving magnetic fluids.

2. MATHEMATICAL FORMULATION

A two-dimensional flow of a couple stress fluid within a channel bounded by parallel plates located at $y = \pm h$ is considered. The channel is saturated with anisotropic porous media and the temperature of channel walls maintained at (T_w), a constant. A magnetic dipole is positioned at a distance $\mathbf{a}$ above the channel wall, exerting an influence on the flow. The walls of the channel, which are assumed to be stretching, induce the flow, with the surface velocity being directly proportional to the horizontal axis X. The porous medium is assumed to be anisotropic, and consequently, the anisotropic permeability matrix $\mathbb{K}$ is defined as [31]–[39]

$$\mathbb{K} = \begin{bmatrix} k_{22}\cos^2(\phi) + k_{11}\sin^2(\phi) & (k_{22} - k_{11})\sin(\phi)\cos(\phi) \\ (k_{22} - k_{11})\sin(\phi)\cos(\phi) & k_{22}\sin^2(\phi) + k_{11}\cos^2(\phi) \end{bmatrix}. \tag{1}$$

k_{11} and k_{22}, the permeabilities along the two main axes are taken to be constant. The angle formed by positive X axis and horizontal permeability k_{22} is the anisotropic angle ϕ. Figure (1) depicts the above consideration. The governing equations for couple stress fluid with consideration of anisotropic porous permeability are stated below, taking into account the aforementioned factors:

$$\frac{\partial u}{\partial x} + \frac{\partial v}{\partial y} = 0, \tag{2}$$

$$\begin{aligned} \rho\Big[u\frac{\partial u}{\partial x} + v\frac{\partial u}{\partial y}\Big] = &-\frac{\partial p}{\partial x} + \mu\Big[\frac{\partial^2 u}{\partial x^2} + \frac{\partial^2 u}{\partial y^2}\Big] - \gamma\Big[\frac{\partial^4 u}{\partial x^4} + \frac{\partial^4 u}{\partial y^4} + 2\frac{\partial^4 u}{\partial x^2 \partial y^2}\Big] + \mu_0 M\frac{\partial H}{\partial x} \\ &-\frac{\mu}{k_{11}k_{22}}\Big[(k_{11}\cos^2(\phi) + k_{22}\sin^2(\phi))u + (\frac{k_{11} - k_{22}}{2}\sin(2\phi))v\Big], \end{aligned} \tag{3}$$

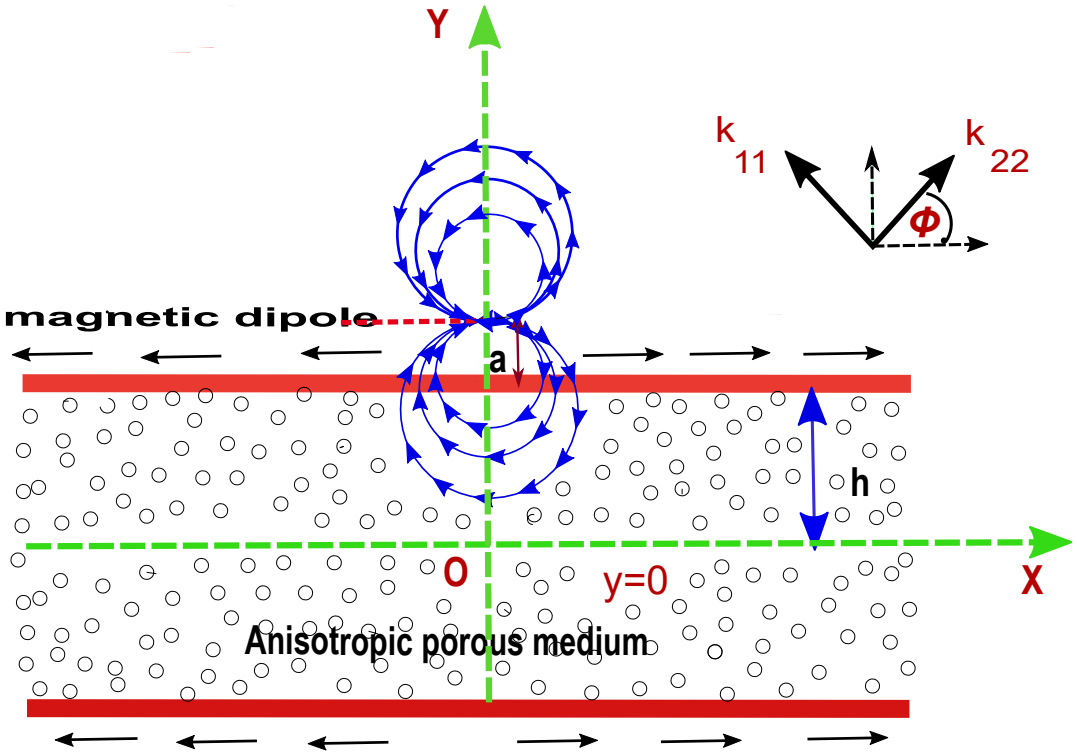

Figure 1. Illustration of physical problem.

$$\rho\Big[u\frac{\partial v}{\partial x}+v\frac{\partial v}{\partial y}\Big]=-\frac{\partial p}{\partial y}+\mu\Big[\frac{\partial^2 v}{\partial x^2}+\frac{\partial^2 v}{\partial y^2}\Big]-\gamma\Big[\frac{\partial^4 v}{\partial x^4}+\frac{\partial^4 v}{\partial y^4}+2\frac{\partial^4 v}{\partial x^2\partial y^2}\Big]+\mu_0 M\frac{\partial H}{\partial y}$$
$$-\frac{\mu}{k_{11}k_{22}}\Big[\frac{k_{11}-k_{22}}{2}\sin(2\phi)u+(k_{11}\sin^2(\phi)+k_{22}\cos^2(\phi))v\Big], \tag{4}$$

$$\rho c_p\Big[u\frac{\partial T}{\partial x}+v\frac{\partial T}{\partial y}\Big]=k\Big[\frac{\partial^2 T}{\partial x^2}+\frac{\partial^2 T}{\partial y^2}\Big]-\mu_0 T\frac{\partial M}{\partial T}\Big[u\frac{\partial H}{\partial x}+v\frac{\partial H}{\partial y}\Big]+\mu\Big[2\left(\frac{\partial u}{\partial x}\right)^2+$$
$$2\left(\frac{\partial v}{\partial y}\right)^2+\left(\frac{\partial u}{\partial y}+\frac{\partial v}{\partial x}\right)^2\Big]+\gamma\Big[\left(\frac{\partial^2 u}{\partial x^2}+\frac{\partial^2 u}{\partial y^2}\right)^2+\left(\frac{\partial^2 v}{\partial x^2}+\frac{\partial^2 v}{\partial y^2}\right)^2\Big]+ \tag{5}$$
$$\frac{\mu}{k_{11}k_{22}}\big[(k_{11}\cos^2(\phi)+k_{22}\sin^2(\phi))u^2+(k_{11}-k_{22})\sin(2\phi)uv$$
$$+(k_{22}\cos^2(\phi)+k_{11}\sin^2(\phi))v^2\big].$$

In the context of the flow problem, the boundary conditions can be mathematically expressed as:

$$\frac{\partial u}{\partial y}=0,\ v=0,\ \frac{\partial T}{\partial y}=0,\ \text{at } y=0, \tag{6}$$

$$\frac{\partial^2 u}{\partial y^2}=0,\ u=cx,\ v=0,\ T=T_w,\ p+\frac{1}{2}\rho(u^2+v^2)=0 \text{ at } y=h. \tag{7}$$

In equations aforementioned variables u, v represent fluid velocity's dimensional components in the direction of X, Y axes. Additionally p, μ_0, μ, ρ, γ, k, H, M, T and c_p denotes the pressure, magnetic permeability, dynamic viscosity, bio-magnetic fluid density, couple stress coefficient, thermal conductivity, magnetic field strength, magnetisation, temperature and fluid's specific heat respectively. In equations (3) and (4), the terms $\mu_0 M\frac{\partial H}{\partial x}$, $\mu_0 M\frac{\partial H}{\partial y}$ on the right side represent the magnetic field's influence in fluid flow, the terms $\gamma\left[\frac{\partial^4 u}{\partial x^4}+\frac{\partial^4 u}{\partial y^4}+2\frac{\partial^4 u}{\partial x^2\partial y^2}\right]$, $\gamma\left[\frac{\partial^4 v}{\partial x^4}+\frac{\partial^4 v}{\partial y^4}+2\frac{\partial^4 v}{\partial x^2\partial y^2}\right]$ reflect the internal frictional forces within the fluid and additional couple stresses of the fluid which lead to higher order stress effects that are crucial for accurately describing behavior of non-Newtonian fluids, and the last terms in the equations reflect the Darcy resistance to flow due to the porous medium, modulated by its anisotropic permeability characteristics. In equation (5), the term $\mu_0 T\frac{\partial M}{\partial T}\left[u\frac{\partial H}{\partial x}+v\frac{\partial H}{\partial y}\right]$, represents the magneto-caloric effect, where the magnetic field influences the distribution of temperature and heat transfer in fluid.

The biomagnetic fluid flow is influenced by magnetic dipole which produces a magnetic field. The scalar potential that represents the magnetic force field is given by:

$$\Phi(x,y) = \frac{\alpha}{2\pi}\left[\frac{x}{x^2+(y-b)^2}\right] \tag{8}$$

where $b = a + h$ and α represents the strength of magnetic force field at the point $(0, b)$. The elements corresponding to the magnetic field intensity H are :

$$H_x = -\frac{\partial\Phi}{\partial x} = \frac{\alpha}{2\pi}.\frac{x^2-(y-b)^2}{[x^2+(y-b)^2]^2} \tag{9}$$

$$H_y = -\frac{\partial\Phi}{\partial y} = \frac{\alpha}{2\pi}.\frac{2x(y-b)}{[x^2+(y-b)^2]^2} \tag{10}$$

The resultant magnitude of intensity of magnetic field is

$$H = \sqrt{H_x^2+H_y^2} = \frac{\alpha}{2\pi.[x^2+(y-b)^2]} \tag{11}$$

$$\frac{\partial H}{\partial x} = -\frac{\alpha}{2\pi}.\frac{2x}{(y-b)^4} \tag{12}$$

considering only x and neglecting higher powers

$$\frac{\partial H}{\partial y} = \frac{\alpha}{2\pi}.\Big[-\frac{2}{(y-b)^3}+\frac{4x^2}{(y-b)^5}\Big] \tag{13}$$

Magnetisation M, is shown to be a function of temperature T and exhibits linear variation according to the principle of FHD[40]. Thus we consider $M = k_f T$, where k_f is the pyromagnetic constant.

2.1. Transformation of equations

We present the following dimensionless variables:

$$\Psi(\xi,\eta) = ch^2\xi f(\eta) \tag{14}$$

$$P(\xi,\eta) = \frac{p}{\rho c^2 h^2} = -P_1(\eta) - \xi^2 P_2(\eta), \tag{15}$$

$$\theta(\xi,\eta) = \frac{T}{T_w} = \theta_1(\eta) + \xi^2\theta_2(\eta), \tag{16}$$

$$\xi(x) = \frac{x}{h} \tag{17}$$

$$\eta(y) = \frac{y}{h} \tag{18}$$

where $\Psi(\xi,\eta), P(\xi,\eta), \theta(\xi,\eta)$ are the stream function, the pressure function and the temperature function respectively. Non-dimensionalization of u, v can be made as :

$$u = \frac{\partial\Psi}{\partial y} = ch\xi f'(\eta) \tag{19}$$

$$v = -\frac{\partial\Psi}{\partial x} = -chf(\eta) \tag{20}$$

The continuity equation is clearly satisfied by the variables u and v. After equations (14)- (20) are substituted in equations (3)-(5), and thereafter equating the coefficients of ξ^0, ξ, and ξ^2, we derive the subsequent equations:

$$-\frac{1}{\Gamma^2}f^V + f''' + Re[ff'' - (f')^2] + 2ReP_2 - \frac{2\beta\theta_1}{Re(\eta-d)^4} - \frac{1}{Da}\Big[K\cos^2(\phi)+\sin^2(\phi))\Big]f'(\eta) = 0, \tag{21}$$

$$\frac{1}{\Gamma^2}f^{IV} - f'' - Reff' + ReP_1' - \frac{2\beta\theta_1}{Re(\eta-d)^3} + \frac{1}{Da}\Big[K\sin^2(\phi)+\cos^2(\phi))\Big]f(\eta) = 0, \tag{22}$$

$$ReP_2' + \frac{4\beta\theta_1}{Re(\eta-d)^5} - \frac{2\beta\theta_2}{Re(\eta-d)^3} = 0 \tag{23}$$

$$\theta_1'' + 2\theta_2 + RePrf\theta_1' - \frac{2\lambda\beta(\theta_1)f}{(\eta-d)^3} + \frac{\lambda}{\Gamma^2}(f'')^2 + 4Re\lambda(f')^2 + \frac{1}{Da}\lambda Re[\cos^2(\phi) + K\sin^2(\phi)]f^2 = 0 \tag{24}$$

$$\begin{aligned}\theta_2'' - RePr[2f'\theta_2 - f\theta_2'] + \lambda\beta\theta_1\left[\frac{2f'}{(\eta-d)^4} + \frac{4f}{(\eta-d)^5}\right] - \frac{2\lambda\beta f\theta_2}{(\eta-d)^3} + \lambda\frac{1}{\Gamma^2}(f''')^2 + \lambda Re(f'')^2 \\ + \frac{1}{Da}\lambda Re[K\cos^2(\phi) + \sin^2(\phi)]f^2 = 0.\end{aligned} \tag{25}$$

The boundary conditions in equations (6) and (7) get transformed as:

$$\begin{aligned}&f(0) = 0,\ f''(0) = 0,\ \theta_1'(0) = 0,\ \theta_2'(0) = 0 \\ &f(1) = 0, f'(1) = 1, f'''(1) = 0,\ \theta_1(1) = 1,\ \theta_2(1) = 0,\ P_1(1) = 0,\ P_2(1) = \frac{1}{2}.\end{aligned} \tag{26}$$

In the transformed equations written above, the other non-dimensional parameters present are outlined as follows:

$$\Gamma = \sqrt{\frac{\mu}{\gamma}}h,\ \beta = \frac{\alpha\mu_0 T_w \rho k_f}{2\pi\mu^2},\ Pr = \frac{\mu c_p}{k},\ \lambda = \frac{\mu^2 c}{\rho k_f T_w},$$
$$Da = \frac{k_{11}}{h^2},\ Re = \frac{\rho c h^2}{\mu},\ d = \frac{b}{h}\ and\ K = \frac{k_{11}}{k_{22}}.$$

where the couple stress parameter is denoted as Γ, ferromagnetic interaction parameter as β, Prandtl number as Pr, viscous dissipation parameter as λ, Darcy number as Da, Reynolds number as Re, dimensionless distance as d, and anisotropic permeability ratio as K.

3. METHOD OF SOLUTION

A fifth-order coupled nonlinear system is established by the sets of equations (21)–(25) together with the boundary conditions (26). This system characterises the dynamics of the problem under consideration. A numerical solution to the problem considered is obtained by applying the Spectral Quasi-Linearization Method. For the set of equations (21) to (25), the approximate current solution and the improved solution are considered as f_r, $(\theta_1)_r$, $(\theta_2)_r$, $(P_1)_r$, $(P_2)_r$ and f_{r+1}, $(\theta_1)_{r+1}$, $(\theta_2)_{r+1}$, $(P_1)_{r+1}$, $(P_2)_{r+1}$ respectively. The procedure yields the linear differential equations shown below:

$$a_{1,r}f_{r+1}^V + f_{r+1}''' + a_{2,r}f_{r+1}'' + a_{3,r}f_{r+1}' + a_{4,r}f_{r+1} + a_{5,r}(\theta_1)_{r+1} + a_{6,r}(P_2)_{r+1} = S_1, \tag{27}$$

$$a_{7,r}f_{r+1}^{IV} - f_{r+1}'' + a_{8,r}f_{r+1}' + a_{9,r}f_{r+1} + a_{10,r}(\theta_1)_{r+1} + a_{11,r}(P_1)_{r+1}' = S_2, \tag{28}$$

$$a_{12,r}(\theta_1)_{r+1} + a_{13,r}(\theta_2)_{r+1} + a_{14,r}(P_2)_{r+1}' = S_3, \tag{29}$$

$$a_{15,r}f_{r+1}'' + a_{16,r}f_{r+1}' + a_{17,r}f_{r+1} + (\theta_1)_{r+1}'' + a_{18,r}(\theta_1)_{r+1}' + a_{19,r}(\theta_1)_{r+1} + a_{20,r}(\theta_2)_{r+1} = S_4, \tag{30}$$

$$a_{21,r}f_{r+1}''' + a_{22,r}f_{r+1}'' + a_{23,r}f_{r+1}' + a_{24,r}f_{r+1} + a_{25,r}(\theta_1)_{r+1} + (\theta_2)_{r+1}'' + a_{26,r}(\theta_2)_{r+1}' + a_{27,r}(\theta_2)_{r+1} = S_5, \tag{31}$$

The transformed boundary conditions are found as below:

$$\begin{aligned}&f_{r+1} = 0,\ f_{r+1}'' = 0,\ (\theta_1)_{r+1}' = 0,\ (\theta_2)_{r+1}' = 0\ \text{ at }\ \eta = 0, \\ &f_{r+1} = 0,\ f_{r+1}' = 1,\ f_{r+1}''' = 0,\ (\theta_1)_{r+1} = 1,\ (\theta_2)_{r+1} = 0,\ (P_1)_{r+1} = 0,\ (P_2)_{r+1} = \frac{1}{2}\ \text{ at }\ \eta = 1.\end{aligned} \tag{32}$$

The coefficients obtained are:

$$a_{1,r} = -\frac{1}{\Gamma^2},\quad a_{2,r} = Ref_r,\quad a_{3,r} = -2Ref_r' - \frac{1}{Da}(K\cos^2(\phi) + \sin^2(\phi)),\quad a_{4,r} = Ref_r'',$$
$$a_{5,r} = \frac{-2\beta}{Re(\eta-d)^4},\quad a_{6,r} = 2Re,\quad a_{7,r} = \frac{1}{\Gamma^2},\quad a_{8,r} = -Ref,$$
$$a_{9,r} = -Ref_r' + \frac{1}{Da}(\cos^2(\phi) + K\sin^2(\phi)),\quad a_{10,r} = \frac{-2\beta}{(\eta-d)^3},\quad a_{11,r} = Re,$$
$$a_{12,r} = \frac{4\beta}{(\eta-d)^5},\quad a_{13,r} = \frac{-2\beta}{(\eta-d)^3},\quad a_{14,r} = Re,\quad a_{15,r} = \frac{2\lambda f_r''}{\Gamma^2},\quad a_{16,r} = 8Re\lambda f_r',$$
$$a_{17,r} = RePr\theta_1' - \frac{2\lambda\beta\theta_1}{(\eta-d)^3} + \frac{2}{Da}\lambda f_r Re[\cos^2(\phi) + K\sin^2(\phi)],\quad a_{18,r} = RePrf_r,$$
$$a_{19,r} = \frac{-2\beta\lambda f_r}{(\eta-d)^3},\quad a_{20,r} = 2,\quad a_{21,r} = 2\lambda\frac{1}{\Gamma^2}f_r''',\quad a_{22,r} = 2\lambda Ref_r'',$$

$$a_{23,r} = \frac{2}{Da}\lambda Re f_r'[(K\cos^2(\phi)+\sin^2(\phi))] + \frac{2\lambda\beta\theta_1}{(\eta-d)^4} - 2RePr\theta_2,$$
$$a_{24,r} = RePr(\theta_2')_r - \frac{2\lambda\beta(\theta_2)_r}{(\eta-d)^3} + \frac{4\lambda\beta(\theta_1)_r}{(\eta-d)^5}, \quad a_{25,r} = \frac{2\lambda\beta f_r'}{(\eta-d)^4} + \frac{4\lambda\beta f_r}{(\eta-d)^5},$$
$$a_{26,r} = RePr f_r, \quad a_{27,r} = -2RePr f_r' - \frac{2\lambda\beta f_r}{(\eta-d)^3},$$
$$S_1 = Re(f_r f_r'' - f_r'^2), \quad S_2 = -Re f_r f_r', \quad S_3 = 0,$$
$$S_4 = RePr f_r\theta_1' - \frac{2\lambda\beta f_r\theta_1}{(\eta-d)^3} + 4Re\lambda f_r'^2 + \frac{\lambda f_r''^2}{\Gamma^2} + \frac{\lambda Re}{Da}[\cos^2(\phi)+K\sin^2(\phi)]f_r^2,$$
$$S_5 = -2RePr f_r'(\theta_2)_r + RePr f_r(\theta_2')_r - \frac{2\lambda\beta f_r(\theta_2)_r}{(\eta-d)^3} + \frac{2\lambda\beta f_r'(\theta_1)_r}{(\eta-d)^4} + \frac{4\lambda\beta(\theta_1)_r f_r}{(\eta-d)^5}$$
$$+ \lambda\frac{1}{\Gamma^2}(f_r''')^2 + Re\lambda(f_r'')^2 + \frac{\lambda Re}{Da}[\cos^2(\phi)+K\sin^2(\phi)]f_r'^2.$$

To solve the linearised equations (21) to (25), a Chebyshev spectral collocation approach is used. Chebyshev interpolating polynomials are used to estimate the functions unknown. The Gauss-Lobatto points are defined as $\zeta_j = \cos(\pi j/N)$, where $j = 1, 2, \cdots N$ of collocation points at which these polynomials are collocated. Derivatives of $f(\eta)$, $\theta_1(\eta)$, $\theta_2(\eta)$, $P_1(\eta)$, and $P_2(\eta)$ are determined by using the differential matrix $\mathbf{D}$ to calculate Chebyshev polynomials at the collocation points. Near collocation nodes the derivatives of f_{r+1}, $(\theta_1)_{r+1}$, $(\theta_2)_{r+1}$, $(P_1)_{r+1}$, and $(P_2)_{r+1}$ are represented as:

$$\begin{aligned}
\frac{\partial^p f_{r+1}}{\partial\eta^p} &= \left(\frac{2}{L}\right)^p \sum_{i=0}^{N} D_{N,i}^p f_{r+1}(\eta_i) = \mathbf{D}^p F,\\
\frac{\partial^p (\theta_1)_{r+1}}{\partial\eta^p} &= \left(\frac{2}{L}\right)^p \sum_{i=0}^{N} D_{N,i}^p (\theta_1)_{r+1}(\eta_i) = \mathbf{D}^p \Theta_1,\\
\frac{\partial^p (\theta_2)_{r+1}}{\partial\eta^p} &= \left(\frac{2}{L}\right)^p \sum_{i=0}^{N} D_{N,i}^p (\theta_2)_{r+1}(\eta_i) = \mathbf{D}^p \Theta_2,\\
\frac{\partial^p (P_1)_{r+1}}{\partial\eta^p} &= \left(\frac{2}{L}\right)^p \sum_{i=0}^{N} D_{N,i}^p (P_1)_{r+1}(\eta_i) = \mathbf{D}^p \mathbf{P}_1,\\
\frac{\partial^p (P_2)_{r+1}}{\partial\eta^p} &= \left(\frac{2}{L}\right)^p \sum_{i=0}^{N} D_{N,i}^p (P_2)_{r+1}(\eta_i) = \mathbf{D}^p \mathbf{P}_2.
\end{aligned} \tag{33}$$

where the Chebyshev differentiation matrix $\mathbf{D}$ scaled by $L/2$, is of order $(M+1)\times(M+1)$ with p derivative order. On substituting equation(33) into equations (27)- (31), we obtain

$$[a_{1,r}\mathbf{D}^5 + \mathbf{D}^3 + a_{2,r}\mathbf{D}^2 + a_{3,r}\mathbf{D} + a_{4,r}I]f_{r+1} + a_{5,r}(\theta_1)_{r+1} + a_{6,r}(P_2)_{r+1} = S_1, \tag{34}$$
$$[a_{7,r}\mathbf{D}^4 - \mathbf{D}^2 + a_{8,r}\mathbf{D} + a_{9,r}I]f_{r+1} + [a_{10,r}I](\theta_1)_{r+1} + a_{11,r}\mathbf{D}(P_1)_{r+1} = S_2, \tag{35}$$
$$a_{12,r}(\theta_1)_{r+1} + a_{13,r}(\theta_2)_{r+1} + a_{14,r}\mathbf{D}(P_2)_{r+1} = S_3 \tag{36}$$
$$[a_{15,r}\mathbf{D}^2 + a_{16,r}\mathbf{D} + a_{17,r}I]f_{r+1} + [\mathbf{D}^2 + a_{18,r}\mathbf{D} + a_{19,r}I](\theta_1)_{r+1} + [a_{20,r}I](\theta_2)_{r+1} = S_4, \tag{37}$$
$$[a_{21,r}\mathbf{D}^3 + a_{22,r}\mathbf{D}^2 + a_{23,r}\mathbf{D} + a_{24,r}I]f_{r+1} + a_{25,r}(\theta_1)_{r+1} + [\mathbf{D}^2 + a_{26,r}\mathbf{D} + a_{27,r}I](\theta_2)_{r+1} = S_5. \tag{38}$$

Applying spectral method on the boundary conditions gives:

$$\begin{aligned}
f_{r+1}(\zeta_0) = 0, \ \sum_{k=0}^{N}\mathbf{D}_{N,k}f_{r+1}(\zeta_0) = 1,\\
f_{r+1}(\zeta_N) = 0, \ \sum_{k=0}^{N}\mathbf{D}_{N,k}^2 f_{r+1}(\zeta_N) = 1, \ \sum_{k=0}^{N}\mathbf{D}_{N,k}^3 f_{r+1}(\zeta_0) = 0,\\
\sum_{k=0}^{N}\mathbf{D}_{N,k}(\theta_1)_{r+1}(\zeta_N) = 0, \ \sum_{k=0}^{N}\mathbf{D}_{N,k}(\theta_2)_{r+1}(\zeta_N) = 0, \ (\theta_1)_{r+1}(\zeta_0) = 1, \ (\theta_2)_{r+1}(\zeta_0) = 0,\\
(P_1)_{r+1}(\zeta_0) = 0, \ (P_2)_{r+1}(\zeta_0) = \frac{1}{2}.
\end{aligned} \tag{39}$$

The matrix form of the aforementioned equation system is written as

$$\begin{bmatrix} \mathbf{B}_{11} & \mathbf{B}_{12} & \mathbf{B}_{13} & \mathbf{B}_{14} & \mathbf{B}_{15} \\ \mathbf{B}_{21} & \mathbf{B}_{22} & \mathbf{B}_{23} & \mathbf{B}_{24} & \mathbf{B}_{25} \\ \mathbf{B}_{31} & \mathbf{B}_{32} & \mathbf{B}_{33} & \mathbf{B}_{34} & \mathbf{B}_{35} \\ \mathbf{B}_{41} & \mathbf{B}_{42} & \mathbf{B}_{43} & \mathbf{B}_{44} & \mathbf{B}_{45} \\ \mathbf{B}_{51} & \mathbf{B}_{52} & \mathbf{B}_{53} & \mathbf{B}_{54} & \mathbf{B}_{55} \end{bmatrix} \times \begin{bmatrix} F_{r+1} \\ \Theta_{1r+1} \\ \Theta_{2r+1} \\ P_{1r+1} \\ P_{2r+1} \end{bmatrix} = \begin{bmatrix} S_1 \\ S_2 \\ S_3 \\ S_4 \\ S_5 \end{bmatrix}, \tag{40}$$

The boundary conditions are placed on the separate matrices as follows:

$$\mathbf{B}_{11} = \begin{bmatrix} 1 & 0 & \cdots & 0 & 0 \\ \mathbf{D}_{1,0} & \mathbf{D}_{1,1} & \cdots & \mathbf{D}_{1,N-1} & \mathbf{D}_{1,N} \\ \mathbf{D}^{\mathbf{3}}_{\mathbf{2,0}} & \mathbf{D}^{\mathbf{3}}_{\mathbf{2,1}} & \cdots & \mathbf{D}^{\mathbf{3}}_{\mathbf{2,N-1}} & \mathbf{D}^{\mathbf{3}}_{\mathbf{2,N}} \\ \hline & & B_{11} & & \\ \hline \mathbf{D}^{\mathbf{2}}_{\mathbf{N-1,0}} & \mathbf{D}^{\mathbf{2}}_{\mathbf{N-1,1}} & \cdots & \mathbf{D}^{\mathbf{2}}_{\mathbf{N-1,N-1}} & \mathbf{D}^{\mathbf{2}}_{\mathbf{N-1,N}} \\ 0 & 0 & \cdots & 0 & 1 \end{bmatrix}, \quad \mathbf{B}_{12} = \begin{bmatrix} 0 & 0 & \cdots & 0 & 0 \\ 0 & 0 & \cdots & 0 & 0 \\ 0 & 0 & \cdots & 0 & 0 \\ \hline & & B_{12} & & \\ \hline 0 & 0 & \cdots & 0 & 0 \\ 0 & 0 & \cdots & 0 & 0 \end{bmatrix},$$

$$\mathbf{B}_{13} = \begin{bmatrix} 0 & 0 & \cdots & 0 & 0 \\ 0 & 0 & \cdots & 0 & 0 \\ 0 & 0 & \cdots & 0 & 0 \\ \hline & & B_{13} & & \\ \hline 0 & 0 & \cdots & 0 & 0 \\ 0 & 0 & \cdots & 0 & 0 \end{bmatrix}, \quad \mathbf{B}_{14} = \begin{bmatrix} 0 & 0 & \cdots & 0 & 0 \\ 0 & 0 & \cdots & 0 & 0 \\ 0 & 0 & \cdots & 0 & 0 \\ \hline & & B_{14} & & \\ \hline 0 & 0 & \cdots & 0 & 0 \\ 0 & 0 & \cdots & 0 & 0 \end{bmatrix}, \quad \mathbf{B}_{15} = \begin{bmatrix} 0 & 0 & \cdots & 0 & 0 \\ 0 & 0 & \cdots & 0 & 0 \\ 0 & 0 & \cdots & 0 & 0 \\ \hline & & B_{15} & & \\ \hline 0 & 0 & \cdots & 0 & 0 \\ 0 & 0 & \cdots & 0 & 0 \end{bmatrix},$$

$$\mathbf{B}_{21} = \begin{bmatrix} 0 & 0 & \cdots & 0 & 0 \\ \hline & & B_{21} & & \\ \hline 0 & 0 & \cdots & 0 & 0 \end{bmatrix}, \quad \mathbf{B}_{22} = \begin{bmatrix} 1 & 0 & \cdots & 0 & 0 \\ \hline & & B_{22} & & \\ \hline \mathbf{D}_{N,0} & \mathbf{D}_{N,1} & \cdots & \mathbf{D}_{N,N-1} & \mathbf{D}_{N,N} \end{bmatrix},$$

$$\mathbf{B}_{23} = \begin{bmatrix} 0 & 0 & \cdots & 0 & 0 \\ \hline & & B_{23} & & \\ \hline 0 & 0 & \cdots & 0 & 0 \end{bmatrix}, \quad \mathbf{B}_{24} = \begin{bmatrix} 0 & 0 & \cdots & 0 & 0 \\ \hline & & B_{24} & & \\ \hline 0 & 0 & \cdots & 0 & 0 \end{bmatrix}, \quad \mathbf{B}_{25} = \begin{bmatrix} 0 & 0 & \cdots & 0 & 0 \\ \hline & & B_{25} & & \\ \hline 0 & 0 & \cdots & 0 & 0 \end{bmatrix},$$

$$\mathbf{B}_{31} = \begin{bmatrix} 0 & 0 & \cdots & 0 & 0 \\ \hline & & B_{31} & & \\ \hline 0 & 0 & \cdots & 0 & 0 \end{bmatrix}, \quad \mathbf{B}_{32} = \begin{bmatrix} 0 & 0 & \cdots & 0 & 0 \\ \hline & & B_{32} & & \\ \hline 0 & 0 & \cdots & 0 & 0 \end{bmatrix}, \quad \mathbf{B}_{33} = \begin{bmatrix} 1 & 0 & \cdots & 0 & 0 \\ \hline & & B_{33} & & \\ \hline \mathbf{D}_{N,0} & \mathbf{D}_{N,1} & \cdots & \mathbf{D}_{N,N-1} & \mathbf{D}_{N,N} \end{bmatrix},$$

$$\mathbf{B}_{34} = \begin{bmatrix} 1 & 0 & \cdots & 0 & 0 \\ \hline & & B_{34} & & \\ \hline 0 & 0 & \cdots & 0 & 1 \end{bmatrix}, \quad \mathbf{B}_{35} = \begin{bmatrix} 1 & 0 & \cdots & 0 & 0 \\ \hline & & B_{35} & & \\ \hline 0 & 0 & \cdots & 0 & 1 \end{bmatrix}, \quad \mathbf{B}_{41} = \begin{bmatrix} 0 & 0 & \cdots & 0 & 0 \\ \hline & & B_{41} & & \\ \hline 0 & 0 & \cdots & 0 & 0 \end{bmatrix},$$

$$\mathbf{B}_{42} = \begin{bmatrix} 0 & 0 & \cdots & 0 & 0 \\ \hline & & B_{42} & & \\ \hline 0 & 0 & \cdots & 0 & 0 \end{bmatrix}, \mathbf{B}_{43} = \begin{bmatrix} 0 & 0 & \cdots & 0 & 0 \\ \hline & & B_{43} & & \\ \hline 0 & 0 & \cdots & 0 & 0 \end{bmatrix}, \quad \mathbf{B}_{44} = \begin{bmatrix} 1 & 0 & \cdots & 0 & 0 \\ \hline & & B_{44} & & \\ \hline 0 & 0 & \cdots & 0 & 0 \end{bmatrix},$$

$$\mathbf{B}_{45} = \begin{bmatrix} 0 & 0 & \cdots & 0 & 0 \\ \hline & & B_{45} & & \\ \hline 0 & 0 & \cdots & 0 & 0 \end{bmatrix}, \mathbf{B}_{51} = \begin{bmatrix} 0 & 0 & \cdots & 0 & 0 \\ \hline & & B_{51} & & \\ \hline 0 & 0 & \cdots & 0 & 0 \end{bmatrix}, \quad \mathbf{B}_{52} = \begin{bmatrix} 0 & 0 & \cdots & 0 & 0 \\ \hline & & B_{52} & & \\ \hline 0 & 0 & \cdots & 0 & 0 \end{bmatrix},$$

$$\mathbf{B}_{53} = \begin{bmatrix} 0 & 0 & \cdots & 0 & 0 \\ \hline & & B_{53} & & \\ \hline 0 & 0 & \cdots & 0 & 0 \end{bmatrix}, \mathbf{B}_{54} = \begin{bmatrix} 0 & 0 & \cdots & 0 & 0 \\ \hline & & B_{54} & & \\ \hline 0 & 0 & \cdots & 0 & 0 \end{bmatrix}, \quad \mathbf{B}_{55} = \begin{bmatrix} 1 & 0 & \cdots & 0 & 0 \\ \hline & & B_{55} & & \\ \hline 0 & 0 & \cdots & 0 & 0 \end{bmatrix},$$

$$\mathbf{F}_{r+1} = \begin{bmatrix} f_{r+1,0} \\ f_{r+1,1} \\ \hline \vdots \\ \hline f_{r+1,N-2} \\ f_{r+1,N-1} \\ f_{r+1,N} \end{bmatrix}, \mathbf{\Theta_1}_{r+1} = \begin{bmatrix} \theta_{1r+1,0} \\ \hline \vdots \\ \vdots \\ \hline \theta_{1r+1,N} \end{bmatrix}, \quad \mathbf{\Theta_2}_{r+1} = \begin{bmatrix} \theta_{2r+1,0} \\ \hline \vdots \\ \vdots \\ \hline \theta_{2r+1,N} \end{bmatrix}, \quad \mathbf{P}_{1r+1} = \begin{bmatrix} P_{1r+1,0} \\ \hline \vdots \\ \vdots \\ \hline 0 \end{bmatrix},$$

$$P_{2r+1} = \begin{bmatrix} \mathbf{P}_{2r+1,0} \\ \hline \vdots \\ \vdots \\ \hline 0 \end{bmatrix}, S_1 = \begin{bmatrix} 0 \\ 1 \\ 0 \\ \hline \\ \mathbf{s_1} \\ \hline 1 \\ 0 \end{bmatrix}, \quad S_2 = \begin{bmatrix} 0 \\ \hline \\ \mathbf{s_2} \\ \hline 1 \end{bmatrix}, \quad S_3 = \begin{bmatrix} 0 \\ \hline \\ \mathbf{s_3} \\ \hline 0 \end{bmatrix}, \quad S_4 = \begin{bmatrix} 0 \\ \hline \\ \mathbf{s_4} \\ \hline 0 \end{bmatrix}, \quad S_5 = \begin{bmatrix} \frac{1}{2} \\ \hline \\ \mathbf{s_5} \\ \hline 0 \end{bmatrix},$$

where

$$\begin{aligned}
&B_{11} = [\text{diag}(\mathbf{a}_{1,r}) \quad 1 \quad \text{diag}(\mathbf{a}_{2,r}) \quad \text{diag}(\mathbf{a}_{3,r}) \quad \text{diag}(\mathbf{a}_{4,r})][\mathbf{D}^5 \quad \mathbf{D}^3 \quad \mathbf{D}^2 \quad \mathbf{D} \quad I]^T,\\
&B_{12} = \text{diag}(\mathbf{a}_{5,r}), \quad B_{13} = 0, \quad B_{14} = 0, \quad B_{15} = \text{diag}(\mathbf{a}_{6,r}),\\
&B_{21} = [\text{diag}(\mathbf{a}_{7,r}) - 1 \quad \text{diag}(\mathbf{a}_{8,r}) \quad \text{diag}(\mathbf{a}_{9,r})][\mathbf{D}^4 \quad \mathbf{D}^2 \quad \mathbf{D} \quad I]^T,\\
&B_{22} = \text{diag}(\mathbf{a}_{10,r}), \quad B_{23} = 0, \quad B_{24} = [\text{diag}(\mathbf{a}_{11,r})]\mathbf{D}, \quad B_{25} = 0,\\
&B_{31} = 0, \quad B_{32} = \text{diag}(\mathbf{a}_{12,r}), \quad B_{33} = [\text{diag}(\mathbf{a}_{13,r}), \quad B_{34} = 0, \quad B_{35} = [\text{diag}(\mathbf{a}_{14,r})][\mathbf{D}],\\
&B_{41} = [\text{diag}(\mathbf{a}_{15,r}) \quad \text{diag}(\mathbf{a}_{16,r}) \quad \text{diag}(\mathbf{a}_{17,r})][\mathbf{D}^2 \quad \mathbf{D} \quad I]^T,\\
&B_{42} = [1 \quad \text{diag}(\mathbf{a}_{18,r}) \quad \text{diag}(\mathbf{a}_{19,r})][\mathbf{D}^2 \quad \mathbf{D} \quad I]^T, \; B_{43} = \text{diag}(\mathbf{a}_{20,r}), \quad B_{44} = 0, \quad B_{45} = 0,\\
&B_{51} = [\text{diag}(\mathbf{a}_{21,r}) \quad \text{diag}(\mathbf{a}_{22,r}) \quad \text{diag}(\mathbf{a}_{23,r}) \quad \text{diag}(\mathbf{a}_{24,r})][\mathbf{D}^3 \quad \mathbf{D}^2 \quad \mathbf{D} \quad I]^T, \; B_{52} = \text{diag}(\mathbf{a}_{25,r}),\\
&B_{53} = [1 \quad \text{diag}(\mathbf{a}_{26,r}) \quad \text{diag}(\mathbf{a}_{27,r})][\mathbf{D}^2 \quad \mathbf{D} \quad I]^T, \quad B_{54} = 0, \quad B_{55} = 0,
\end{aligned}$$

where $\mathbf{a}$, I, 0 are diagonal, unit, and null matrices, respectively, of order (N + 1)×(N + 1).

4. CONVERGENCE ANALYSIS AND RESULTS

Convergence analysis entails demonstrating that the iterative approach converges to an exact solution for the non-linear system of equations (21) and (25), by taking boundary conditions (26) into account. The calculation of residual errors is performed to guarantee the precision of the numerical results. Inaccuracies measure the extent of discrepancy between the numerical and the precise original solution. These errors quantify the degree of deviation experienced by the numerical solution from the original solution. For equations (27) and (29), the residual errors obtained are as follows:

$$\begin{aligned}
Res(f) = &-\frac{1}{\Gamma^2} f^V + f''' + Re[ff'' - (f')^2] + 2ReP_2 - \frac{2\beta\theta_1}{Re(\eta - d)^4} \\
&- \frac{1}{Da}\Big[(K\cos^2(\phi) + \sin^2(\phi))\Big] f'(\eta),
\end{aligned} \tag{41}$$

$$\begin{aligned}
Res(\theta_1) = &\theta_1'' + 2\theta_2 + RePrf\theta_1' - \frac{2\lambda\beta(\theta_1)f}{(\eta - d)^3} + \frac{\lambda}{\Gamma^2}(f'')^2 + 4Re\lambda(f')^2 \\
&+ \frac{1}{Da}\lambda Re[\cos^2(\phi) + K\sin^2(\phi)] f^2.
\end{aligned} \tag{42}$$

$\|Res(f)\|_\infty$, $\|Res(\theta_1)\|_\infty$, are the infinity norms (or maximum norm) of equations (41) and (42), which quantify the largest absolute value of the error throughout the domain. The impact of increasing the count of collocation points (N) on the accuracy of the solution produced by the SQLM (Spectral Quasi-linearization Method) is examined in Fig (2). In figure 2(a), the residual error in f over 30 iterations for various numbers of collocation points (N = 25, 30, 35) is displayed. Collocation points between 25 and 35 yield the best accuracy, with residual errors of about 10^{-6}. Similarly, for the residual error in θ_1 that is shown in 2(b), the ideal residuals are obtained with values of about 10^{-9}. The accuracy

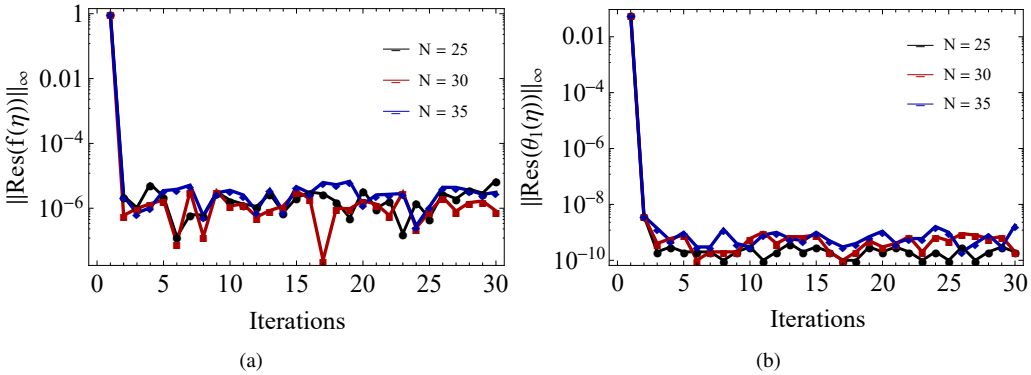

Figure 2. Influence of iterations on (a) $\|Res(f(\eta))\|_\infty$ and (b) $\|Res(\theta_1)\|_\infty$ for collocation points when $\Gamma = 2$, $d = 2$, β = 5, λ = 0.01, $Da = 1$, $Pr = 1$, $K = 0.05$, $\phi = \pi/4$, $Re = 1$.

steadily decreases after this range of collocation points. According to these findings, the numerical approach achieves maximum accuracy with 30-35 collocation points and performs optimally after the fifth iteration. Beyond this range, the accuracy is observed to decrease, as the number of collocation points are increased, and the residual errors stabilise at values that suggest optimal convergence.

Theoretical estimates of the influence of couple stress parameter, ferromagnetic interaction parameter, anisotropic permeability ratio, anisotropic angle, Reynolds number, Darcy number, and Prandtl number on the distributions of velocity and temperature have been determined. Additionally, the influence of β and Pr on the distribution of pressure is also determined. Figures in (3) - (5) depict the variation of the dimensionless axial velocity $f'(\eta)$ for a given cross-section η of channel for different parameters. In figure 3(a), it is observed that higher values of Γ lead to an increase of axial velocity up to a certain height and a slow decrease towards the upper channel wall. An increase of couple stress parameter leads to increase in viscosity, thereby reducing the flow of fluid, and also indicates that the wider the channel, the smaller the magnitude of velocity. This is consistent with the concept that the couple stress fluids experience additional resistance or internal friction due to microstructural interactions. From figure 3(b), it can be noticed that higher values of ferromagnetic

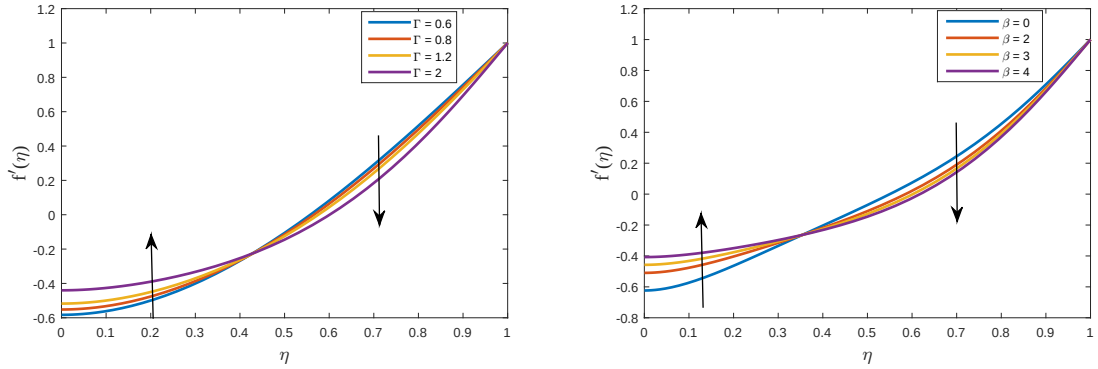

Figure 3. Axial velocity profile for different values of (a) Couple stress parameter Γ (b) Ferromagnetic interaction parameter β for Γ = 3, $d = 2$, β = 5, λ = 0.2, $Da = 0.01$, $Pr = 1$, $K = 0.005$, ϕ = π/4, $Re = 1$.

interaction parameter β lead to an increase in velocity up to a certain height, after which it reduces. A magnetic force generated by an applied magnetic field opposes the fluid motion. Figures in (4) illustrate the impact of K and Da on $f'(\eta)$, the axial velocity. Figure 4(a) depicts a reduction in magnitude of velocity with a rise in values of anisotropic ratio $K = k_{11}/k_{22}$ and fixed $Da(< 1)$ towards the upper boundary. As anticipated, for a given Da, increasing the permeability ratio K lowers the permeability in the flow direction and consequently, declines the velocity's magnitude. Figure 4(b) illustrates that higher values of Da result in a decrease of velocity in vicinity of the center line and then gradually increase from the centre line towards the upper boundary. When Darcy number is high, viscous effects dominate inertial effects which result in decrease of fluid's total velocity. Figures in (5) depict the impacts of ϕ, Pr, and Re upon axial velocity. The profile of axial velocity for various anisotropic angles ϕ is illustrated in figure 5(a). Optimal velocity is attained

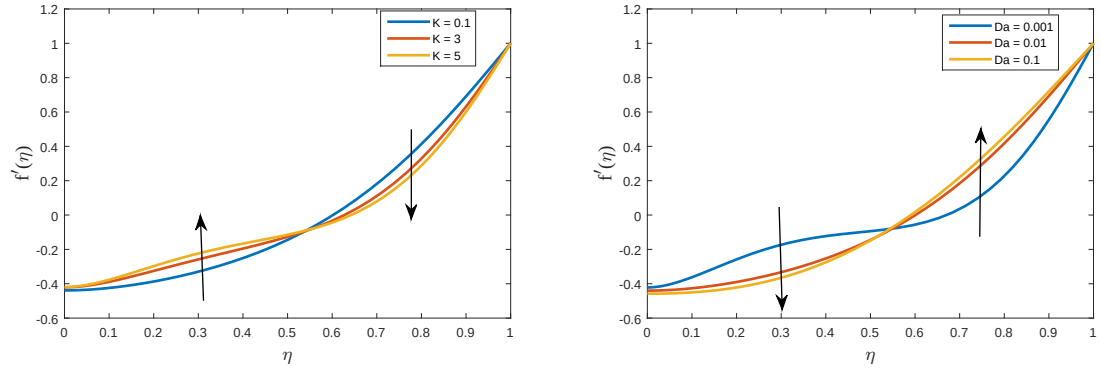

(a) (b)

Figure 4. Axial velocity profile for different values of (a) Anisotropic permeability ratio K (b) Darcy number Da for Γ = 2, $d = 2$, β = 5, λ = 0.2, $Da = 0.01$, $Pr = 1$, $K = 0.005$, ϕ = π/4, $Re = 1$.

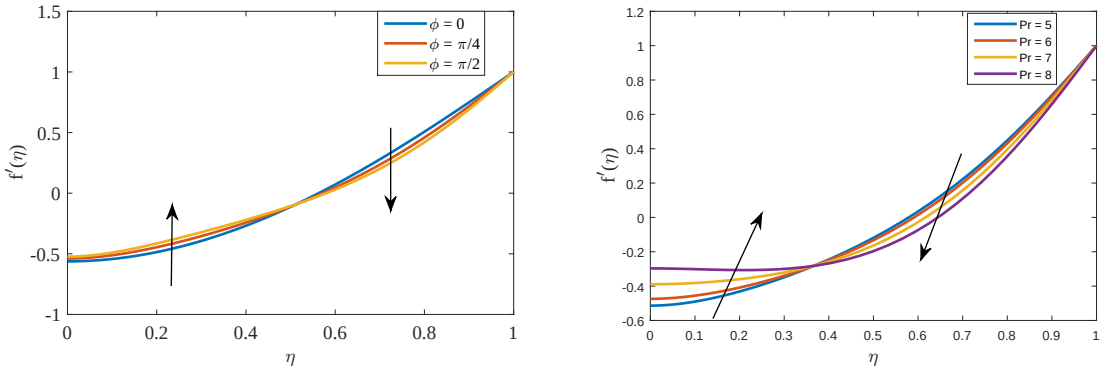

(a) (b)

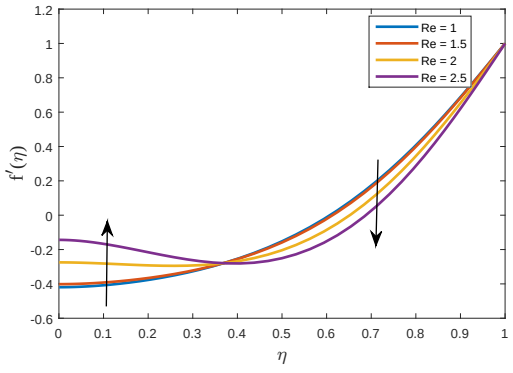

(c)

Figure 5. Axial velocity profile for different values of (a) Anisotropic angle ϕ (b) Prandtl number Pr for Γ = 2, $d = 2$, β = 1, λ = 0.2, $Da = 0.01$, $Pr = 1$, $K = 0.005$, ϕ = π/4, $Re = 0.5$ (c) Reynolds number Re for Γ = 2, $d = 2$, β = 5, λ = 0.2, $Da = 0.01$, $Pr = 2$, $K = 0.005$, ϕ = π/4.

when $\phi = 0$, while the lowest velocity is seen when $\phi = \frac{\pi}{2}$. This behaviour is consistent with the concept that when the value of K is less than or equal to 1 and keeps Da or k_{11} constant, a value of $\phi = 0$ indicates a higher horizontal permeability k_{22}. Conversely, if the value of K is greater than 1, the behaviour will be the opposite. The value of $\phi = 0$ is equivalent to k_{22} the horizontal permeability, resulting in the permeability to reduce in the flow direction. With an increase in values of anisotropic angle, velocity increases up to a certain height and then decreases towards the upper wall. In figure 5(b), up to a certain channel height, axial velocity is noticed to increase and decrease thereafter towards the boundary with an increase of Prandtl number Pr. Prandtl number Pr is a dimensionless number that charaterises the relative thickness of the boundary layers formed by both momentum and heat. Fluid accelerates more effectively within a thicker momentum boundary layer. Figure 5(c) illustrates the increase of velocity up to a certain height and a gradual decrease towards the upper wall, as Reynolds number Re increases. The magnetic force exerts a substantial influence on the flow near the vicinity of magnetic field within a channel, leading to reduction in velocity. Figures (6)-(7) illustrate the

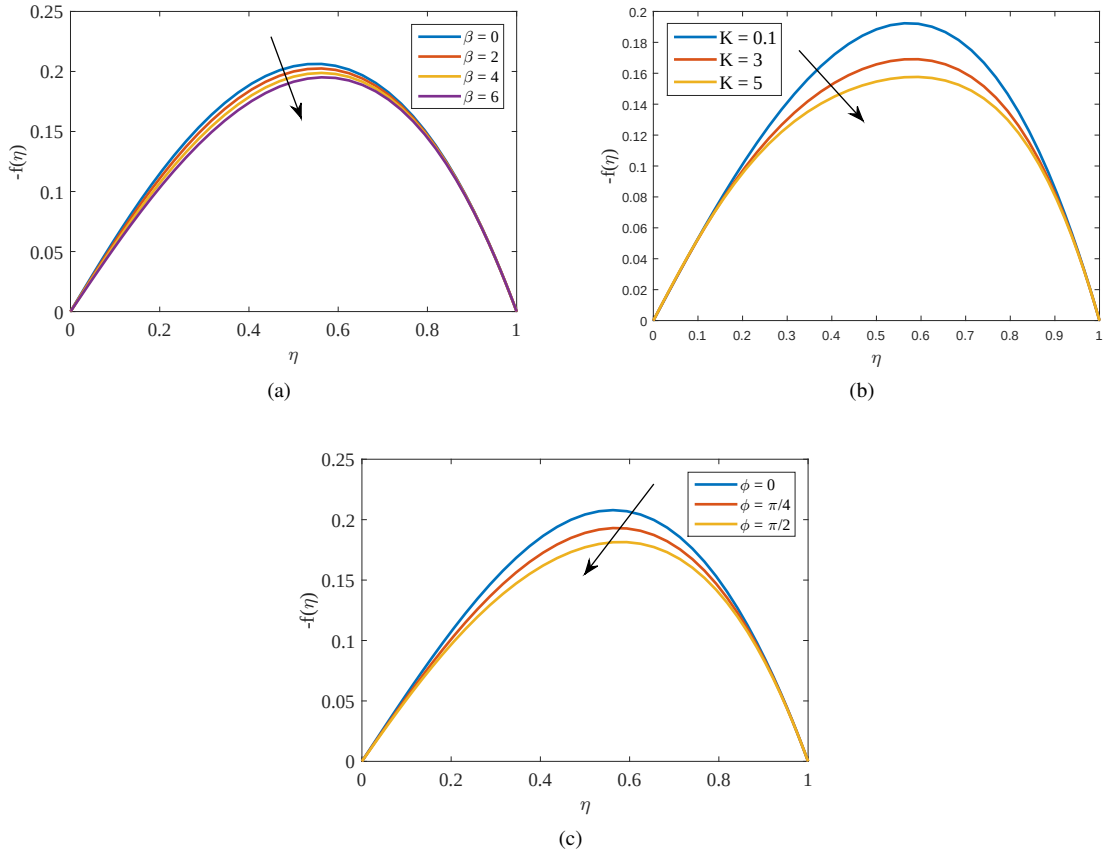

Figure 6. Transverse velocity profile for different values of (a) Ferromagnetic interaction parameter β (b) Anisotropic permeability ratio K (c) Anisotropic angle ϕ for Γ = 2, $d = 2$, β = 5, λ = 0.2, $Da = 0.01$, $Pr = 5$, $K = 0.005$, ϕ = π/4, $Re = 2$.

distribution of dimensionless transverse velocity $-f(\eta)$ for different values of β, K, ϕ, Γ, and Re. Figure 6(a) depicts that transverse velocity decreases with increasing values of β. Transverse motion is reduced when β increases because it strengthens the relation between ferromagnetic particles and the magnetic field. In practical situations, this phenomenon controls the motion and stability of magnetic fluids. In figure 6(b) the velocity is seen reducing for higher values of anisotropic permeability ratio K. For a fixed Da (fixed k_{11}), an increase in K implies a reduction or decrease in k_{22} the horizontal permeability. As k_{22} decreases, the shear resistance increases in the horizontal direction, thereby increasing the dissipation of energy due to internal friction in the flow. This energy dissipation affects the overall reduction of the momentum of fluid and indirectly, the transverse velocity also. In figure 6(c) the velocity is seen reducing for higher values of anisotropic angle ϕ. Elevating anisotropic angle ϕ has dampening effect on velocity, which may be due to permeability ratio K and magnetic parameter that inhibits the flow. Figure 7(a) shows that higher values of Γ result in reduction of velocity. The decrease in transverse velocity within a fluid is due to the increased rotational resistance experienced by the fluid. Figure 7(b), demonstrates a reduction in transverse velocity as the Prandtl number Pr is increased. This phenomenon is because the higher momentum diffusivity compared to thermal diffusivity amplifies thermal gradients and buoyancy effects, resulting in stronger convective currents in the transverse direction. Moreover, the increased viscosity

aids in maintaining these lateral movements. Figure 7(c) illustrates that higher values of Reynolds number Re lead to a reduction in velocity. Generally this is due to the growing influence of inertia in the flow. This leads to a stabilisation in the primary flow direction and a decrease in contribution of viscous forces that facilitate transverse motion.

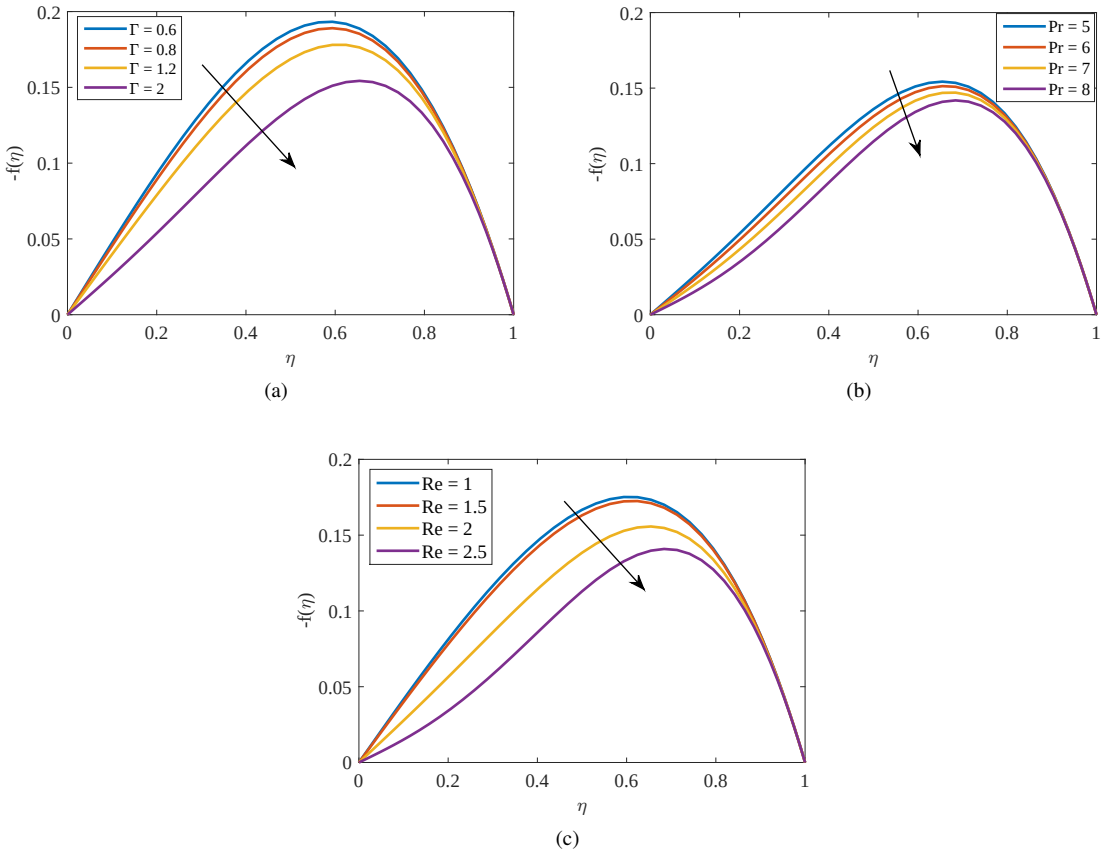

Figure 7. Transverse velocity profile for different values of (a) Couple stress parameter Γ (b) Prandtl number Pr (c) Reynolds number Re for $\Gamma = 2$, $d = 2$, $\beta = 5$, $\lambda = 0.2$, $Da = 0.01$, $Pr = 5$, $K = 0.005$, $\phi = \pi/4$, $Re = 0.5$.

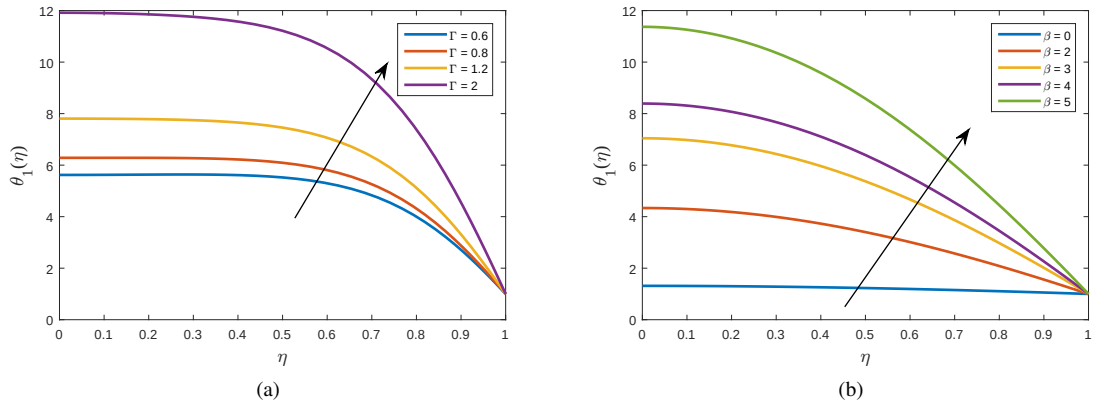

Figure 8. Temperature profile for different values of (a) Couple stress parameter Γ for $d = 2$, $\beta = 1$, $\lambda = 0.2$, $Da = 0.01$, $Pr = 1$, $K = 0.005$, $\phi = \pi/4$, $Re = 21$ (b) Ferromagnetic interaction parameter β for $\Gamma = 2$, $d = 2$, $\lambda = 0.2$, $Da = 0.01$, $Pr = 1$, $K = 0.005$, $\phi = \pi/4$, $Re = 0.01$.

The variation of temperature profile for different parameters is illustrated in figures (8)-(10). Figure 8(a) illustrates that higher values of couple stress parameter Γ result in an increase in temperature. A greater temperature gradient

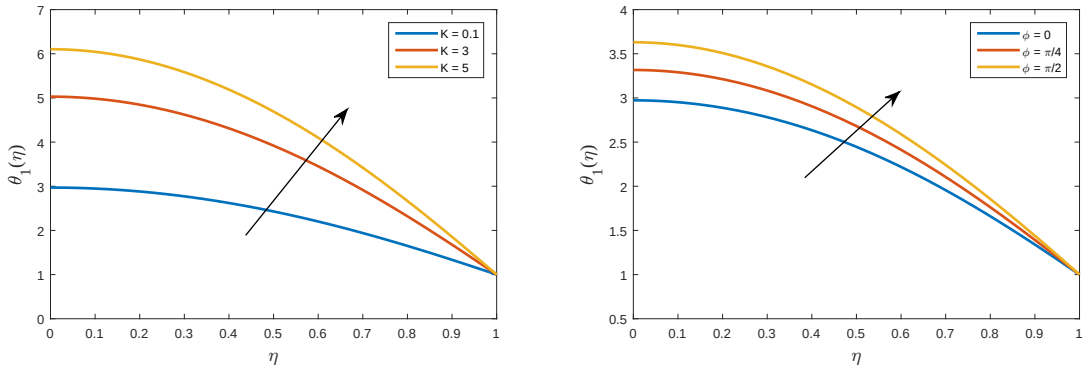

Figure 9. Temperature profile for different values of (a) Anisotropic permeability ratio K (b) Anisotropic angle ϕ for Γ = 2, $d = 2$, β = 1, λ = 0.2, $Da = 0.01$, $Pr = 1$, $K = 0.5$, ϕ = π/4, $Re = 1$.

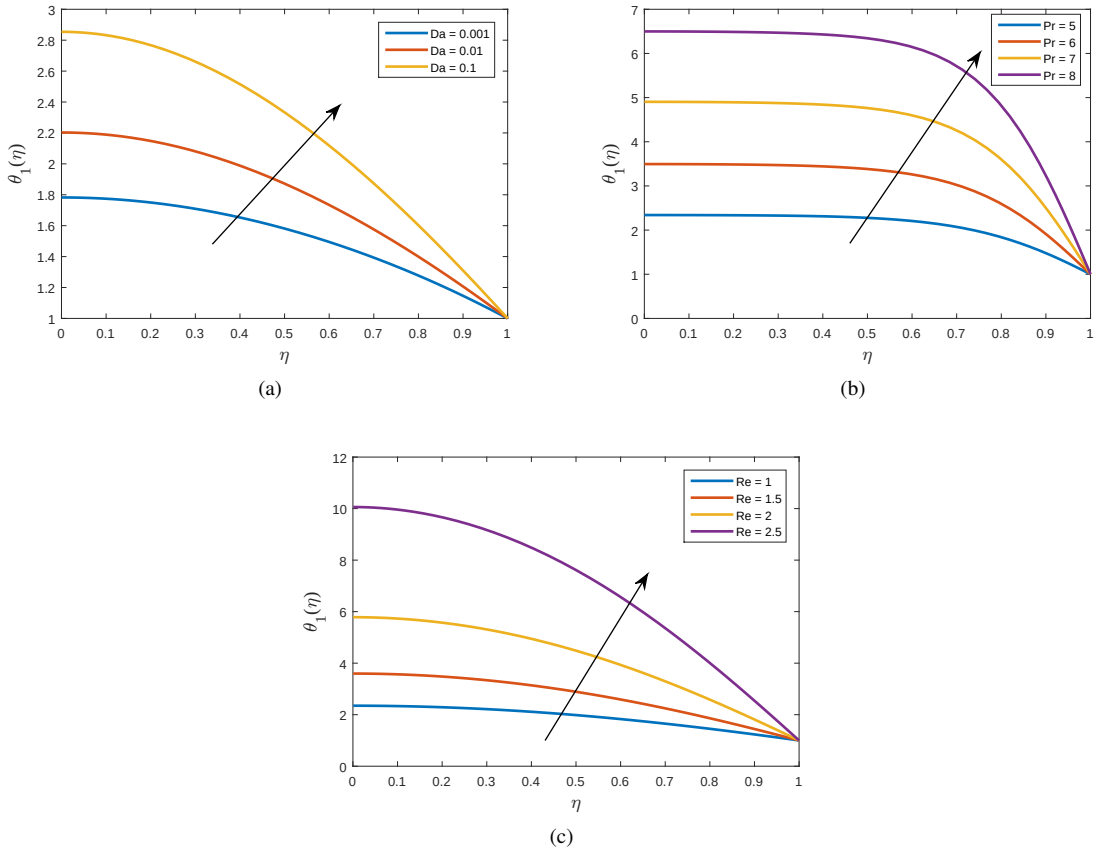

Figure 10. Temperature profile for different values of (a) Darcy number Da (b) Prandtl number Pr (c) Reynolds number Re for Γ = 2, $d = 2$, β = 1, λ = 0.2, $Da = 0.01$, $Pr = 1$, $K = 0.005$, ϕ = π/4, $Re = 0.05$.

results from a thinner thermal boundary layer, which is indicated by a rise in Γ. This leads to enhanced heat transfer at the wall's surface and contributes to the deceleration of fluid. Figure 8(b) depicts an increase of temperature with an increase of ferromagnetic interaction parameter β. A more pronounced temperature difference resulting from an increase in β suggests a reduced thermal boundary layer in close proximity to wall. Enhancement of effective heat transfer from the fluid's surface to its interior occurs at higher values of β. The findings indicate that when the ferromagnetic interaction parameter β is increased, boundary layer temperature and velocity profiles have a significant impact. The findings depicted in figure 8(b) hold significant implications for the management of tumours and cancer therapy, as the aim of hyperthermia is to elevate the temperature of malignant tissues beyond the therapeutic range of 42°C. Plasma protein undergoes irreversible damage when blood temperatures rise above 42°C. Figure 9(a) shows a rise in temperature, with increase in values of K. Increased permeability results in enhanced convection, improved mixing, and consistent temperatures. On the other hand, when permeability is reduced, it limits the movement of fluids, resulting in more pronounced variations in temperature. Figure 9(b) illustrates the increase of temperature when the anisotropic angle ϕ is raised. Figure 10(a) shows that higher Da values typically correspond to more permeable media, allowing for more efficient heat transfer. Figures 10(b) and 10(c) show that higher values of Prandtl number Pr and Reynolds number Re lead to an increase in temperature. A high Pr value, exceeding 5, suggests that fluid momentum is a more advantageous means of heat transfer compared to thermal diffusion. Stated differently, a large Pr value suggests that fluid momentum, rather than fluid conduction, is more prone to induce heat transfer. An illustration of the pressure profile variation for

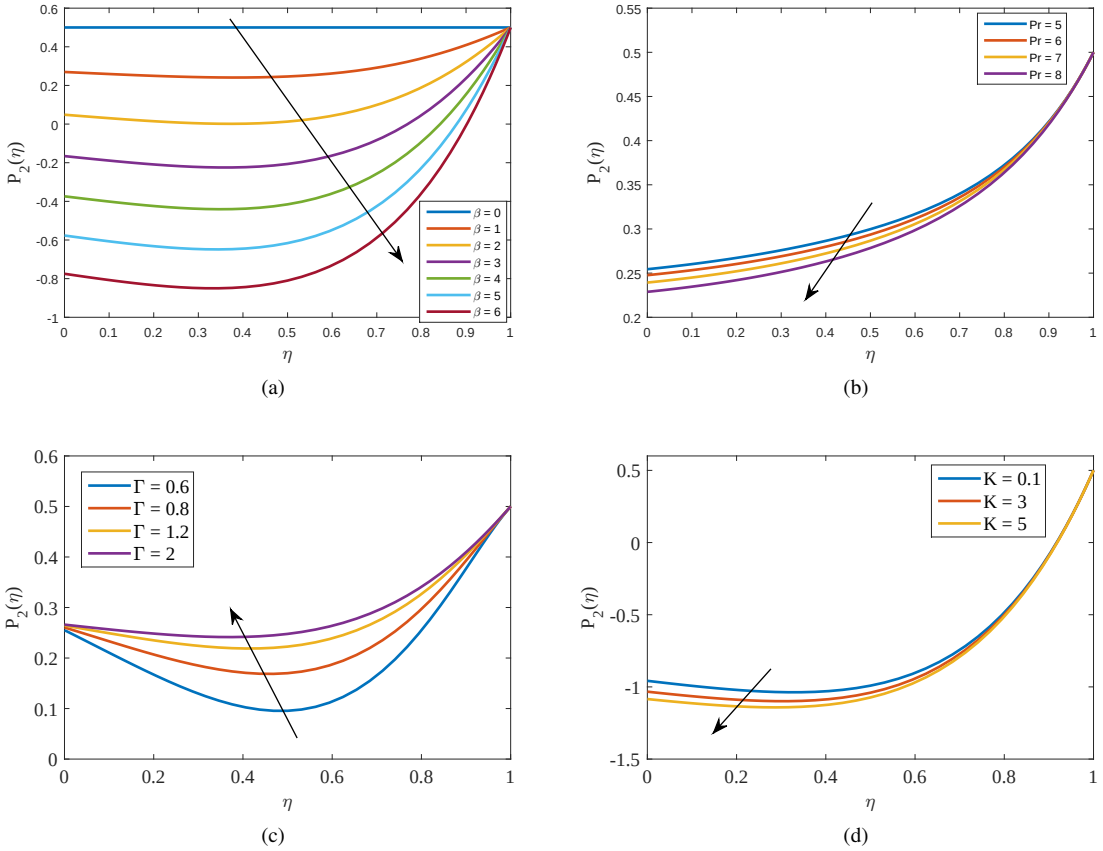

Figure 11. Pressure profile for different values of (a) Ferromagnetic interaction parameter β (b) Prandtl number Pr (c) Couple stress parameter Γ (d) Anisotropic permeability ratio K for $\Gamma = 2$, $d = 2$, $\beta = 7$, $\lambda = 0.2$, $Da = 0.1$, $Pr = 1$, $K = 0.5$, $\phi = \pi/2$, $Re = 2$.

different values of β, Pr, Γ, and K can be seen in figure (11). This figure demonstrates that higher values of β, Pr, and K result in pressure drops while a rise in pressure when Γ is increased. Hypothetical findings in figure 11(a) are highly relevant for clinical interventions, where the application of a suitably powerful magnetic force field can be utilized to control blood pressure. As the fluid resists both thermal and momentum diffusion more strongly, higher values of Pr (fig.11(b)) generally lead to greater pressure drops across the channel, so increasing the overall resistance to flow. In figure 11(c), we observe the rise in pressure with an increase of Γ. The pressure profile can be noticed to be flattened, indicating less and smoother variation. Figure 11(d) depicts a decline in pressure as the values of K are increased which suggests a more streamlined flow and maximum pressure can be noticed at the upper boundary wall. The parameters of

local skin friction and rate of heat transfer are essential for the analysis of flow and heat transfer. The following relations are used to define these quantities:

$$C_f = \frac{\tau_\omega}{\rho c^2 x^2}, \quad Nu_x = \frac{x}{T_w}\frac{\partial T}{\partial y}|_{y=1} \tag{43}$$

Using equations (16-20) in equation (43) we get:

$$C_f Re_x^{\frac{1}{2}} = [f''(1) - \frac{1}{\Gamma^2} f''''(1)], \qquad Nu_x Re_x^{\frac{-1}{2}} = (\theta_1'(1) + \xi^2 \theta_2'(1)) \tag{44}$$

In the above equations $\tau_\omega = \left[\mu(\frac{\partial u}{\partial y}) - \gamma(\frac{\partial^3 u}{\partial y^3})\right]_{y=1}$ represents shear stress at wall, Nu_x is local Nusselt number, and $Re_x = \frac{\rho c x^2}{\mu}$ is local Reynolds number. Also $\theta'(1) = (\theta_1'(1) + \xi^2\theta_2'(1))$ is the dimensionless heat transfer parameter at wall. It is evident that the ferromagnetic interaction parameter β has an impact on the flow field. However, the flow problem is separated from the thermal energy problem in the hydrodynamic case (β=0), where P_2 becomes constant and zero (See Equations (23) and (26)). Therefore it is more intriguing and practical to replace the dimensionless wall heat transfer parameter $\theta'(1) = (\theta_1'(1) + \xi^2\theta_2'(1))$ by the ratio $\theta^*(1) = \frac{\theta_1'(1)}{\theta_1'(1)|_{\beta=0}}$ which is dimensionless and independent of ξ and represents coefficient of heat transfer rate at the wall.

Γ	$f''(1) - \frac{1}{\Gamma^2} f''''(1)$					
	β=0	β=3	β=5	β=7	β=9	$\beta = 11$
0.2	123.3324773	127.257181	129.8463308	132.4148978	134.9635621	137.4935335
0.3	56.6660337	59.61461236	61.56274982	63.49615971	65.41650618	67.32454648
0.4	33.333494	35.93842135	37.65954421	39.36947234	41.06914359	42.75847324
0.5	22.53442963	24.97755792	26.59253685	28.19715192	29.79325785	31.38089637
1	8.140794606	10.34148191	11.79708708	13.24627189	14.69095588	16.13263003
10	3.433573507	5.00769968	6.06391105	7.133794256	8.219453759	9.322318935
100	3.292810745	4.83203191	5.871098686	6.930397385	8.012385729	9.118768452

Table 1. Distribution of dimensionless wall shear parameter $f''(1) - \frac{1}{\Gamma^2} f''''(1)$

Tables (1) and (2) display variations in Skin friction cofficient and heat transfer rate for different values of Γ and β. The other parameters are maintained at following values: d = 2, λ = 0.2, Da = 0.1, Pr = 1, K = 0.05, $\phi = \pi/4$, Re = 1.

Γ	$\theta^*(1) = \frac{\theta_1'(1)}{\theta_1'(1)\|_{\beta=0}}$				
	β=0	β=3	β=5	β=7	β=9
0.2	-3.4970961551	-3.4986914879	-3.4997561776	-3.5008218082	-3.5018883853
0.3	-1.5708573035	-1.5724195493	-1.5734629036	-1.5745077275	-1.5755540441
0.4	-0.8966478411	-0.8981991396	-0.8992365341	-0.9002764930	-0.9013190138
0.5	-0.5845572012	-0.5861041374	-0.5871404232	-0.5881807258	-0.5892250551
1	-0.1681483019	–0.1696977885	-0.1718171673	-0.1718171673	-0.1729002803
10	-0.0278343318	-0.0299616020	-0.0313761276	-0.0328310790	-0.0343730535

Table 2. Distribution of coefficient of heat transfer rate $\theta^*(1)$

Table (1) presents variations of the local skin friction coefficient for various values of the parameters Γ and β. At the surface, the drag force is decreased by higher couple stress parameters, as Table (1) shows. Microstructural effects of couple stress fluids can reduce the total frictional resistance against fluid flow, producing a smoother fluid motion. Higher values of the ferromagnetic interaction parameter result in an increase in the magnetic force, which acts as a resistive force like drag force, within the fluid. Consequently, the velocity gradient near the wall becomes more pronounced, resulting in an elevation in the shear stresses. Hence the coefficient of skin friction rises with increase of magnetic parameter. The variations in heat transfer rate at channel wall's surface for different values of Γ and β are summarised in Table (2). It can be inferred from this that higher values of Γ lead to an increased heat transfer rate near the surface. For a given Γ, increasing β leads to a reduction in heat transfer rate. The microstructural effects in a couple stress fluids obstruct thermal conductivity and hence reduce heat transfer efficiency. This table supports the conclusion that microstructural effects from couple stress and ferromagnetic interaction parameters significantly influence heat transfer behaviour.

5. CONCLUSION

In this paper, the dynamics of biomagnetic couple stress fluid in a channel with stretchable walls, are analysed. The channel is saturated with an anisotropic porous medium. The governing equations, accounting for couple stresses and magnetic forces, are solved using the Spectral Quasi-Linearization Method (SQLM). To examine how key parameters,

including couple stress, ferromagnetic interaction, Prandtl number, Reynolds number, Darcy number, anisotropic permeability, and angle affect velocity, temperature, and pressure profiles in boundary layers, graphs were created using an in-house developed MATLAB program. The findings are outlined below:

- Couple stress parameter and ferromagnetic interaction parameter significantly impact the flow characteristics of fluid. Higher values of Γ and β lead to a reduction in both axial and transverse velocities and a rise in temperature.
- Higher values of K and ϕ result in a reduction in both axial and transverse velocities and a rise in temperature.
- Higher values of Da indicate less restricted flow, so the axial velocity increases near the upper boundary and the temperature increases.
- A higher Prandtl number Pr results in the decrease of both axial and transverse velocities near the upper boundary and the temperature increases.
- Higher β, Pr, and K values result in pressure drops whereas a rise in Γ leads to a rise in pressure. As the fluid resists both thermal and momentum diffusion more strongly, higher values of Pr generally lead to greater pressure drops across the channel, so increasing the overall resistance to flow.
- Higher values of Γ lead to a reduction in skin friction coefficient and an enhancement in rate of heat transfer.
- Higher values of β result in an enhancement in both skin friction and rate of heat transfer coefficient.

The convergence analysis demonstrated that the SQLM was effective. The velocity and temperature profiles' residual errors showed quick convergence, with accuracy greatly increasing after the fifth iteration. Accuracy was optimal with 25-35 collocation points but gradually declined after that. The numerical method is robust and efficient, as evidenced by residual error norms ranging from 10^{-6} to 10^{-9} for different parameters. Overall, this work fills a gap in the literature by providing in-depth insights into the combined impacts of couple stress fluid dynamics, magnetic dipoles, and anisotropic porous media on fluid flow and heat transfer. The current study offers valuable recommendations for enhancing heat transfer and flow control in engineering applications that involve couple stress ferrofluids.

ORCID

R. Vijaya Sree, https://orcid.org/0009-0002-0047-302X; **V. Krishna Narla**, https://orcid.org/0000-0003-0994-3497; **K. Suresh Babu**, https://orcid.org/0000-0003-1538-1072

REFERENCES

[1] L.J. Crane, "Flow past a stretching plate," Z. Angew. Math. Phys. **21**, 645-647 (1970). https://doi.org/10.1007/BF01587695

[2] R.E. Rosensweig, *Ferrohydrodynamics*, (Cambridge University Press. Cambridge, (1985).

[3] S. Odenbach, *Magnetoviscous Effects in Ferrofluids*, (Springer, Berlin, 2002).

[4] N.H. Abu-Hamdeh, R.A.R. Bantan, F. Aalizadeh, and A. Alimoradi, "Controlled drug delivery using the magnetic nanoparticles in non-Newtonian blood vessels," Alexandria Engineering Journal, **59**, 4819–4828 (2020). https://doi.org/10.1016/j.aej.2020.07.010

[5] M. Kole, and S. Khandekar, "Engineering applications of ferrofluids: A review," Journal of Magnetism and Magnetic Materials, **537**, 168222 (2021). https://doi.org/10.1016/j.jmmm.2021.168222

[6] M.S. Pattanaik, V.B. Varma, S.K. Cheekati, V. Chaudhary, and R.V. Ramanujan, "Optimal ferrofluids for magnetic cooling devices," Scientific Reports, **11**(1), (2021). https://doi.org/10.1038/s41598-021-03514-2

[7] N. Kastor, B. Dandu, V. Bassari, G. Reardon, and Y. Visell, "Ferrofluid electromagnetic actuators for high-fidelity haptic feedback," Sensors and Actuators a Physical, **355**, 114252 (2023). https://doi.org/10.1016/j.sna.2023.114252

[8] E.E. Tzirtzilakis, "A mathematical model for blood flow in magnetic field," Physics of Fluids, **17**(7), (2005). https://doi.org/10.1063/1.1978807

[9] J.C. Misra, G.C. Shit, and H.J. Rath, "Flow and heat transfer of a MHD viscoelastic fluid in a channel with stretching walls: Some applications to haemodynamics," Computers and Fluids, **37**(1), 1–11 (2008). https://doi.org/10.1016/j.compfluid.2006.09.005

[10] Misra, J.C., and Shit, G.C., "Flow of a biomagnetic visco-elastic fluid in a channel with stretching walls," J. Appl. Mech. **76**(6), 061006 (2009). https://doi.org/10.1115/1.3130448.

[11] J.C. Misra, B. Pal, and A.S. Gupta, "Hydromagnetic flow of a second-grade fluid in a channel—Some applications to physiological systems," Math. Models Meth. Appl. Sci. **8**, 1323-1342 (1998). https://doi.org/10.1142/S0218202598000627

[12] V.K. Stokes, "Couple stress in fluids," Phys. Fluids, **9**, 1709-1715 (1966). https://doi.org/10.1063/1.1761925

[13] K. Abbas, X. Wang, G. Rasool, T. Sun, G. Yin, and I. Razzaq, "Recent developments in the application of ferrofluids with an emphasis on thermal performance and energy harvesting," J. Magn. Magn. Mater. **587**, 171311 (2023). https://doi.org/10.1016/j.jmmm.2023.171311

[14] R.K. Shah and S. Khandekar, "Exploring ferrofluids for heat transfer augmentation," J. Magn. Magn. Mater. **475**, 389-400 (2019). https://doi.org/10.1016/j.jmmm.2018.11.034

[15] M. Nandeppanavar, K. Vajravelu, M. Abel, and M.N. Siddalingappa, "Second order slip flow and heat transfer over a stretching sheet with non-linear Navier boundary condition," Int. J. Therm. Sci. **58**, 143-150 (2012). https://doi.org/https://doi.org/10.1016/j.ijthermalsci.2012.02.019

[16] K. Ramesh, "Influence of heat and mass transfer on peristaltic flow of a couple stress fluid through porous medium in the presence of inclined magnetic field in an inclined asymmetric channel," J. Mol. Liq. **219**, 256-271 (2016). https://doi.org/10.1016/j.molliq.2016.03.010

[17] M. Reddy and R.M. Josyula, "Effect of magnetic field on couple stress fluid flow in a rectangular channel," AIP Conf. Proc. **2246**, 020057 (2020). https://doi.org/10.1063/5.0014635

[18] R. Mahesh, A.B. Vishalakshi, U. Mahabaleshwar, and F. Sofos, "Impact of an inclined magnetic field on couple stress fluid flow over a stretching surface with effect of Stefan blowing, radiation and chemical reaction," J. Magn. Magn. Mater. **580**, 170953 (2023). https://doi.org/10.1016/j.jmmm.2023.170953

[19] M. Naveed, M. Imran, and S. Gul, "Heat transfer analysis in hydromagnetic flow of couple stress fluid in presence of homogeneous and heterogeneous chemical reactions over a porous oscillatory stretchable sheet," Adv. Mech. Eng. **15**(2), 16878132231155823 (2023). https://doi.org/10.1177/16878132231155823

[20] H.I. Andersson, K.H. Bech, and B.S. Dandapat, "Magnetohydrodynamic flow of a power-law fluid over a stretching sheet," Int. J. Non-Linear Mech. **27**, 929-936 (1992). https://doi.org/10.1016/0020-7462(92)90045-9

[21] M.A.A. Mahmoud and M.A.E. Mahmoud, "Analytical solutions of hydromagnetic boundary layer flow of a non-Newtonian power-law fluid past a continuously moving surface," Acta Mech. **181**, 83-89 (2006). https://doi.org/10.1007/s00707-005-0268-5

[22] M.Yang, and Y. Lin, "Flow and heat transfer of non-Newtonian power-law fluids over a stretching surface with variable thermal conductivity," Multidiscip. Model. Mater. Struct. **15**(4), 678-695 (2019). https://doi.org/10.1108/MMMS-08-2018-0147

[23] S. Nadeem, R.U. Haq, and C. Lee, "MHD flow of a Casson fluid over an exponentially shrinking sheet," Scientia Iranica, **19**(6), 1550–1553 (2012). https://doi.org/10.1016/j.scient.2012.10.021

[24] P.K. Yadav and N. Yadav, "A study on the flow of couple stress fluid in a porous curved channel," Comput. Math. Appl. **15**2, 1-15 (2023). https://doi.org/10.1016/j.camwa.2023.10.004

[25] M. Ishaq, S.U. Rehman, M.B. Riaz, and M. Zahid, "Hydrodynamical study of couple stress fluid flow in a linearly permeable rectangular channel subject to Darcy porous medium and no-slip boundary conditions," Alexandria Engineering Journal, **91**, 50–69 (2024). https://doi.org/10.1016/j.aej.2024.01.066

[26] S. Das, R.R. Patra, and R.N. Jana, "The layout of Boussinesq couple-stress fluid flow over an exponentially stretching sheet with slip in porous space subject to a variable magnetic field," Multidiscipline Modeling in Materials and Structures, **16**(5), 1131–1154 (2020). https://doi.org/10.1108/MMMS-09-2019-0168

[27] R.A. Alharbey, H. Mondal, and R. Behl, "Spectral Quasi-Linearization Method for Non-Darcy Porous Medium with Convective Boundary Condition," Entropy, **21**(9), 838 (2019). https://doi.org/10.3390/e21090838

[28] H. Mondal and S. Bharti, "Spectral Quasi-linearization for MHD Nanofluid Stagnation Boundary Layer Flow due to a Stretching/Shrinking Surface," J. Appl. Comput. Mech. **6**(4), 1058-1068 (2020). https://doi.org/10.22055/jacm.2020.33097.2207

[29] D. Srinivasacharya, and K.H. Bindu, "Entropy generation in a micropolar fluid flow through an inclined channel with slip and convective boundary conditions," Energy, **91**, 72–83 (2015). https://doi.org/10.1016/j.energy.2015.08.014

[30] K. Raj, B. Moskowitz, and R. Casciari, "Advances in ferrofluid technology," Journal of Magnetism and Magnetic Materials, **149**(1–2), 174–180 (1995). https://doi.org/10.1016/0304-8853(95)00365-7

[31] T. Karmakar, M. Reza, and G.P.R. Sekhar, "Forced convection in a fluid saturated anisotropic porous channel with isoflux boundaries," Physics of Fluids, **31**(11), (2019). https://doi.org/10.1063/1.5126892

[32] T. Karmakar, M. Alam, M. Reza, and G.P.R. Sekhar, "Couette-Poiseuille flow in a fluid overlying an anisotropic porous layer," Comput. Math. Appl. **151**, 346-358 (2023). https://doi.org/10.1016/j.camwa.2023.10.006

[33] N. Ghosh, T. Karmakar, and G.P. Raja Sekhar, "Application of conformal mapping to two-dimensional flows in an anisotropic aquifer," Indian J. Pure Appl. Math. **53**, 617–626 (2022). https://doi.org/10.1007/s13226-021-00153-1

[34] T. Karmakar, and G.P. Raja Sekhar, "A note on flow reversal in a wavy channel filled with anisotropic porous material," Proc. R. Soc. A, **473**, 20170193 (2017). https://doi.org/10.1098/rspa.2017.0193

[35] T. Karmakar, and G. P. Raja Sekhar, "Squeeze-film flow between a flat impermeable bearing and an anisotropic porous bed," Phys. Fluids, **30**, 042001 (2018). https://doi.org/10.1063/1.5020135

[36] T. Karmakar, and G.P. Raja Sekhar, "Effect of anisotropic permeability on fluid flow through composite porous channel," J. Eng. Math. **100**, 33-51 (2016). https://doi.org/10.1007/s10665-015-9831-9

[37] S. Pramanik, and T. Karmakar, "Couette–Poiseuille flow of variable viscosity in a multilayered channel partially filled with a homogeneous anisotropic porous layer: Role of the glycocalyx in attenuating shear stress on endothelial cells," Physics of Fluids, **36**(3), (2024). https://doi.org/10.1063/5.0188683

[38] D.A.S. Rees, L. Storesletten, and A. Postelnicu, "The onset of convection in an inclined anisotropic porous layer with oblique principal axes," Transp. Porous Media, **62**, 139–156 (2006). https://doi.org/10.1007/s11242-005-0618-8

[39] M. Norouzi, and M.R. Shoghi, "A numerical study on miscible viscous fingering instability in anisotropic porous media," Phys. Fluids, **26**, 084102 (2014). https://doi.org/10.1063/1.4891228

[40] E.E. Tzirtzilakis, N.G. Kafoussias, and P.M. Hatzikonstantinou, "Biomagnetic fluid flow in a 3D rectangular duct," Int. J. Numer. Methods Fluids, **44**(12), 1279-1298 (2004). https://doi.org/10.1002/fld.618

ПОТІК РІДИНИ В УМОВАХ ПОДВІЙНОГО БІОМАГНІТНОГО СТРЕСУ В АНІЗОТРОПНОМУ ПОРИСТОМУ КАНАЛІ З РОЗТЯГНУТИМИ СТІНКАМИ

П. Віджая Срі[a,b], **В. Крішна Нарла**[b*], **К. Суреш Бабу**[c]

[a] *Інженерний коледж ACE, математичний факультет, Хайдарабад, Телангана, 501301, Індія*

[b] *GITAM, факультет математики, Хайдарабад, 502329, Індія*

[c] *Інженерно технологічний інститут Гокараджу Рангараджу, кафедра математики, Гайдарабад, 500090, Індія*

У цій роботі досліджується динаміка потоку рідини в умовах подвійного біомагнітного стресу в анізотропному пористому каналі, де стінки каналу розтягуються. Це дослідження вивчає поведінку потоку під впливом зовнішнього магнітного поля, створюваного магнітним диполем. Для спрощення рівнянь задачі вводяться відповідні безрозмірні параметри. Щоб отримати рішення проблеми, використовується відповідний чисельний підхід, заснований на методі спектральної квазілінеаризації. У цій роботі досліджується вплив кількох важливих параметрів, таких як коефіцієнт анізотропної проникності, параметр парних напруг, анізотропний кут, число Дарсі, параметр феромагнітної взаємодії, число Рейнольдса та число Прандтля. Результати вказують на те, що параметр феромагнітної взаємодії та параметр напруги з'єднання суттєво впливають на теплообмін і потік рідини. Коефіцієнт проникності та кут також впливають на динаміку потоку. Крім того, досліджували коефіцієнт поверхневого тертя та швидкість теплообміну, змінюючи параметри парних напруг та феромагнітної взаємодії. Отримані дані демонструють, що існування магнітного диполя та анізотропної проникності значно впливає на течію та теплові властивості феррорідини, надаючи цінну інформацію для оптимізації теплопередачі та контролю потоку рідини в різноманітних інженерних і медичних застосуваннях.

Ключові слова: *рідина під парним стресом; магнітний диполь; анізотропні пористі середовища; анізотропна проникність; теплообмін; метод спектральної квазілінеаризації*